Environmental Science & Technology

pubs.acs.org/est

Article

Biochar Promotes Arsenopyrite Weathering in Simulated Alkaline Soils: Electrochemical Mechanism and Environmental Implications

Shuai Wang, Peng Liao, Ling Cen, Hongguang Cheng, and Qingyou Liu*

Cite This: *Environ. Sci. Technol.* 2023, 57, 8373−8384

Read Online

ACCESS | Metrics & More | Article Recommendations | Supporting Information

ABSTRACT: Oxidation dissolution of arsenopyrite (FeAsS) is one of the important sources of arsenic contamination in soil and groundwater. Biochar, a commonly used soil amendment and environmental remediation agent, is widespread in ecosystems, where it participates in and influences the redox-active geochemical processes of sulfide minerals associated with arsenic and iron. This study investigated the critical role of biochar on the oxidation process of arsenopyrite in simulated alkaline soil solutions by a combination of electrochemical techniques, immersion tests, and solid characterizations. Polarization curves indicated that the elevated temperature (5−45 °C) and biochar concentration (0−1.2 g·L^{-1}) accelerated arsenopyrite oxidation. This is further confirmed by electrochemical impedance spectroscopy, which showed that biochar substantially reduced the charge transfer resistance in the double layer, resulting in smaller activation energy (E_a = 37.38−29.56 kJ·mol^{-1}) and activation enthalpy (ΔH^* = 34.91−27.09 kJ·mol^{-1}). These observations are likely attributed to the abundance of aromatic and quinoid groups in biochar, which could reduce Fe(III) and As(V) as well as adsorb or complex with Fe(III). This hinders the formation of passivation films consisting of iron arsenate and iron (oxyhydr)oxide. Further observation found that the presence of biochar exacerbates acidic drainage and arsenic contamination in areas containing arsenopyrite. This study highlighted the possible negative impact of biochar on soil and water, suggesting that the different physicochemical properties of biochar produced from different feedstock and under different pyrolysis conditions should be taken into account before large-scale applications to prevent potential risks to ecology and agriculture.

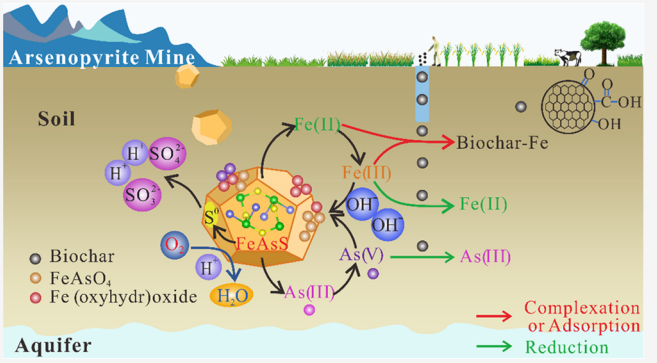

KEYWORDS: *arsenopyrite, biochar, simulated alkaline soils, electrochemical techniques, arsenic contamination*

INTRODUCTION

Arsenic (As) is a toxic trace element that causes various cancers and blood disorders in humans due to long-term chronic exposure.[1] The bioavailability, mobility, and toxicity of As are tightly related to its speciation, in particular, trivalent arsenic is 60 times more toxic than pentavalent.[2] Elevated arsenic in groundwater, surface water, and agricultural soils is a global environmental problem that has threatened the health of millions of people.[3] As-bearing sulfide minerals, e.g., arsenopyrite and As-rich pyrite, and As-rich iron (oxyhydr)oxide are the dominant As-containing geogenic minerals, which are the main minerals responsible for As contamination in the environment through natural activities such as oxidative weathering of minerals or anthropogenic releases of As.[4,5] As the most common As-containing sulfide mineral, the redox dynamic of arsenopyrite significantly affects the geochemical behavior of arsenic.

Biochar is a carbon-rich material originating from pyrolyzing biomass under oxygen-limited conditions, which is used extensively as a soil amendment by enhancing soil fertility, water retention, and mediating soil pH.[6] Such a wide range of applications had led to the prevalence of biochar in nature that can participate in various geochemical processes.[7] It has been demonstrated that biochar is a redox-active substance that can either donate or accept electrons due to the abundance of aromatic and quinoid functional groups, potentially mediating abiotic and biotic reactions. Because biochar can absorb and release hundreds of micrograms of electrons,[8] it can reduce Fe(III), adsorb or complex Fe(III)/Fe(II), thus promoting the reductive dissolution of iron (oxyhydr)oxides and enhancing the release and transport of As.[9−11]

As a semiconductor material, the oxidative dissolution of arsenopyrite is essentially an electrochemical reaction process.[12−14] It has been demonstrated that under near-neutral or even weakly acidic (pH > 4) conditions, the iron released

Received: February 2, 2023
Revised: April 13, 2023
Accepted: May 10, 2023
Published: May 24, 2023

during the oxidation process would rapidly oxidize to iron (oxyhydr)oxides on the mineral surface,[15,16] hindering the oxidation of arsenopyrite. Additionally, the iron arsenate generated by the interaction of arsenic and iron can also passivate the oxidation of arsenopyrite. Furthermore, previous studies have revealed that the low molecular weight organic acids such as citrate can expedite the oxidation of arsenopyrite and As-rich pyrite, alongside with the release of arsenic.[4,17] Further, humic acid has also been proven to promote the biological oxidation of arsenopyrite,[18] while our recent work has confirmed its ability to accelerate abiotic oxidation and mitigate hydrogen ion contamination using electrochemical techniques.[19]

The recent literature reports that soil alkalization has become progressively more severe. Specifically, there are 1 billion hectares of saline soils widely distributed in the world, which are the main cause of land degradation.[20] Emerging research demonstrates that the addition of biochar to saline soils can promote carbon turnover and improved nutrient and chemical properties, as well as land reclamation.[21,22] Furthermore, biochar can be effectively applied to meadow soils for degradation restoration and productivity enhancement.[23] Arsenopyrite polluted alkaline soils are widely distributed in the world and are increasing with mining activities.[24−26] However, the effect of biochar on the oxidation behavior of arsenopyrite in alkaline soils and the fate and transport of Fe and As species that are released during the oxidation process remain unclear.

The objectives of this work were to understand how and to what extent biochar influences the oxidation of arsenopyrite in simulated alkaline soil solutions, as well as the fate and transformation of As and Fe species. To this end, different electrochemical techniques and surface detection methods were used to characterize the oxidative dissolution of arsenopyrite as a function of biochar concentration, alkaline soil type, and temperature. Understanding the mechanism of arsenopyrite oxidation in the presence of biochar, coupled with the fate of As and Fe, can shed light on the possible negative or positive impacts of biochar on soil and environmental ecology quality. The findings gained from this work could also provide practical guidance for electrochemical methods as a new technique for solving environmental problems with similar conductive minerals.

MATERIALS AND METHODS

Mineral Sample. The mineral sample used in this study was obtained from a Carlin-type gold deposit, Guangxi, China. X-ray diffraction (XRD) indicated that the mineral was pure arsenopyrite,[19] and the main composition was approximately 43.56% As, 34.78% Fe, and 20.14% S, as determined by energy dispersive spectroscopy (EDS). The arsenopyrite powder was ground to 200 meshes with an agate mortar and alcohol. After drying in a nitrogen atmosphere, it was sealed in a plastic bag and stored in a vacuum drying box to minimize the oxidation of the powder.

Biochar and Simulated and Real Alkaline Soil Solution Preparation. Biochar was prepared by pyrolyzing wheat straw at a heat treatment temperature of 550 °C. In the pyrolysis process, the heating rate was maintained at 20 °C·min^{-1}, and the holding time was 1 h.[27] Detailed characterizations of the physical and chemical properties of biochar are listed in Table S1 in the Supporting Information (SI). To obtain a homogeneous size of the biochar, an agate mortar and alcohol were used to grind the biochar to 200 meshes. According to the physicochemical properties of meadow soil and saline soil in the "Code for investigation of geotechnical engineering (GB50021-2008)",[28] a simulated alkaline soil (SAS) solution was prepared. The composition of simulated meadow soil included NaCl, Na_2SO_4, and $NaHCO_3$ concentrations of 0.028, 0.19, and 0.11 (g·L^{-1}). Accordingly, the simulated saline soil solution consisted of 1.81 NaCl and 17.74 Na_2SO_4 (g·L^{-1}). The pH of the simulated meadow and saline soil solution was adjusted to 7.4 and 8.6 using H_2SO_4 and NaOH solutions, respectively.[28] In parallel, real meadow and saline soils were collected, and they were performed in electrochemical experiments to compare the results obtained from simulated soil solutions. The pH values of the meadow and saline soils were 7.58 and 8.59, respectively. The content of dissolved organic carbon in the leachate of real meadow and saline soils was 32.48 and 22.27 mg·L^{-1}. Detailed pH test and leachate preparation methods are provided in SI Section S1, and the selected chemical compositions of real soil leachates are shown in Table S2. In this work, two other alkaline solutions were additionally prepared to reveal the reason for the different weathering rates of arsenopyrite in the SAS solution and real soil leachates. Detailed solution preparations are provided in SI Section S2. Analytical grade and deionized water were employed in all experiments.

Electrochemical Methods. An electrochemical workstation (PARSTAT 2273) equipped with a personal computer was used to conduct all electrochemical experiments. A traditional three-electrode cell was used, including an arsenopyrite electrode as the working electrode, platinum auxiliary electrode, and saturated calomel electrode (SCE) as the reference electrode. The surface of the arsenopyrite electrode exposed to the electrolyte was 0.5 cm × 0.5 cm, with an area of 0.25 cm^2. A copper wire was connected to the upper surface of the electrode, and the electrode was sealed with epoxy resin to isolate other surfaces from the environment. Prior to each electrochemical test, the exposed surface was continuously polished with 1000, 3000, and 5000 mesh silicon carbide sandpaper to obtain a mirror-like surface, which helped to ensure the repeatability of the experiment. In this experiment, unless otherwise mentioned, all potentials were relative to the SCE (0.242 V at 25 °C versus standard hydrogen electrode). Electrochemical techniques including cyclic voltammetry (CV), polarization curve, and impedance spectroscopy (EIS) were used to investigate the weathering of arsenopyrite in the SAS solution.

The CV tests were initiated to begin at the open-circuit potential (OCP) in a positive-going direction at 20 mV·s^{-1}. The potential range of the scan was −700 mV to 700 mV. In the polarization curve test, the potential was scanned from −250 mV to 250 mV (versus OCP) at a rate of 10 mV·s^{-1}. EIS experiments were conducted at OCP with 10 mV perturbation in a frequency range of 0.01−10000 Hz and using ZSimpWin 3.20 (2004) to fit the experimental data based on the suitable electrochemical equivalent circuit (EEC). Additional information on electrochemical measurements is provided in SI Section S3. Before each of the above tests, the open circuit potential of the arsenopyrite electrode must be tested first to ensure the stability of the electrode−solution system, and the criterion is that the OCP changes no more than 2.0 mV within 5 min. To ensure reproducibility and stability, all tests were conducted at least in triplicate.

https://doi.org/10.1021/acs.est.2c09874
Environ. Sci. Technol. 2023, 57, 8373−8384

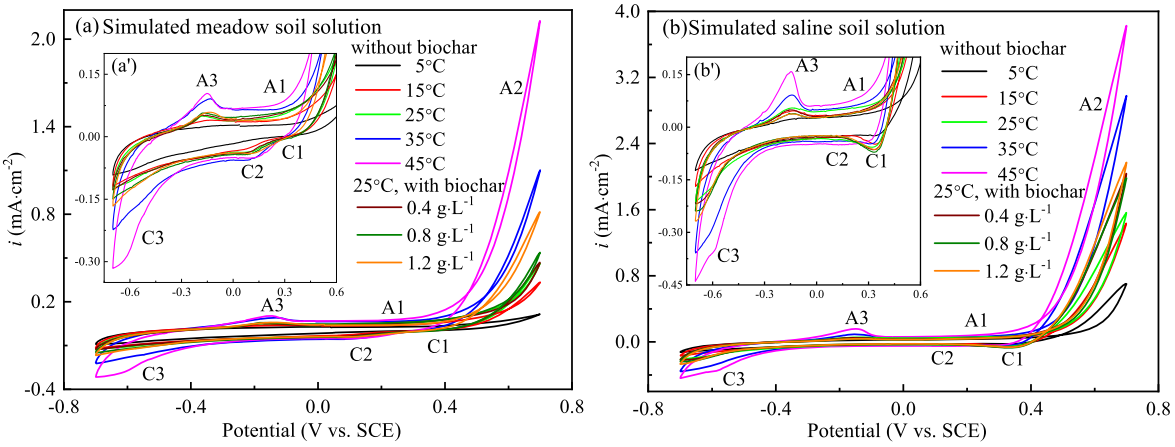

Figure 1. CV for arsenopyrite in simulated alkaline soil solutions at different temperatures and biochar concentrations.

Immersion Experiments. Based on the form of minerals (powder versus block), immersion experiments were conducted to characterize the mineral surface and liquid phase. The powder immersion experiment examined the effects of different temperatures and biochar concentrations on the weathering of arsenopyrite by adding 1 g of arsenopyrite powder and 100 mL of the SAS solution in an Erlenmeyer flask. We set up experiments with different system temperatures to explore the quantitative effects of variations in ambient temperature due to different latitudes and seasons on arsenic release from arsenopyrite. In experiments with temperature as a variable, no biochar was added to the two SAS solutions, and five sets of temperature gradients were set up with temperature as the variable: 5, 15, 25, 35, and 45 °C. Similarly, to investigate the impact of biochar dosage on the oxidative dissolution of arsenopyrite, four SAS solutions containing different biochar concentrations (0, 0.4, 0.8, and 1.2 g·L^{-1}) were set up at 25 °C.

Meanwhile, another set of parallel immersion experiment was set up to examine the changes in the liquid phase of different biochar concentrations in influencing the oxidation of arsenopyrite, such as the species and content changes of As (As(T), As(III)) and Fe (Fe(T), Fe(II)). To further examine the biochar effect obtained in the SAS solution, an additional set of immersion experiments was carried out using real soil leachates with different biochar concentrations, and the change of As(T) content in the liquid phase was monitored. Fe concentrations were determined by a modified ferrozine method.[29] As concentrations were determined by a liquid chromatography-atomic fluorescence spectrometer (LC-AFS 9700). The specific experimental operations and detailed measurement procedures for Fe and As concentrations are provided in SI Section S4.

A pH meter was used to measure the pH changes of the SAS solutions and real soil leachates at 25 °C. In addition, the block immersion test is designed to probe changes in mineral surface morphology after biochar addition. Block arsenopyrite (5 × 5 × 3 mm) was immersed in the SAS solutions at 25 °C with different biochar concentrations (0, 0.4, 0.8, and 1.2 g·L^{-1}).

To verify the adsorption and reduction effect of biochar on Fe(III) as established in the previous literature,[11,30,31] we conducted a separate soaking experiment. Biochar (10 g·L^{-1}) and $Fe_2(SO_4)_3$ (Fe^{3+} = 300 mg·L^{-1}) were placed in a 100 mL Erlenmeyer flask under aerobic conditions, and the content of Fe(II) and Fe(III) in the solution was measured after 24 h using a ferrozine method. To exclude the effect of hydroxide ions on the precipitation of iron ions by simply examining the effect of biochar, the pH of the solution was adjusted to 2.0 in the experiment. Similarly, additional immersion experiments were performed to verify the adsorption and reduction of As(V) by biochar, and the concentrations of As(T) and As(III) in the liquid phase were measured after 24 h of immersion. Besides, another group of immersion test was designed to detect the changes in the structure of biochar before and after contacting with Fe(III) and/or As(V). The experiments were set up in four groups: biochar, biochar + As(V), biochar + Fe(III), and biochar + Fe(III) + As(V). The concentration of biochar was fixed at 2.0 g/L, and the concentration of Fe(III) and As(V) was 4.8 mM, where the pH of the solution was adjusted to 5.0. All immersion experiments were performed at least in duplicate.

Characterization. After being immersed for 80 days, the eroded arsenopyrite powers were analyzed by X-ray photoelectron spectroscopy (XPS, ESCALAB 250XI), and the surface structure of biochar was detected by Fourier transform infrared spectroscopy (FTIR, Bruker Vertex 70). The morphology and composition of blocks were characterized by Raman spectroscopy (British Renishaw) and scanning electron microscopy (SEM, JSM-6460LV). XPS was equipped with an Al Kα radiation source (1486.68 eV), and Avantage 5.948 software was used to fit the peaks. In the process of fitting XPS peaks, all As 3d and S 2p were assigned as doublets that had spin−orbit splitting values of 0.68 and 1.19 eV with intensity ratios of 3:2 and 2:1 and the same full width half-maximum in doublet peaks, respectively. Three peaks were conducted to fit the Fe(II) bonding with As−S, and Fe(III) contained four major multiplet peaks, separating peaks at 0.96 and 1.0 eV, which were based on theoretical core p level multiplet structures for free transition metal ions.[32] The binding energy correction was based on the C1 s peak (284.8 eV). In fitting the XPS spectra, we referred to the data of previous studies.[14,32,33] The range of FTIR spectra was 400−4000 cm^{-1}, and the resolution was 4 cm^{-1}. The Raman instrument was equipped with 50 mW laser power (514 nm), and the acquisition time was 10 s.

RESULTS AND DISCUSSION

Electrochemical Analysis. *Cyclic Voltammetry Study.* Figure 1 shows the CV curve of arsenopyrite in the simulated meadow and saline soil solutions. The similar shape of the

https://doi.org/10.1021/acs.est.2c09874
Environ. Sci. Technol. 2023, 57, 8373−8384

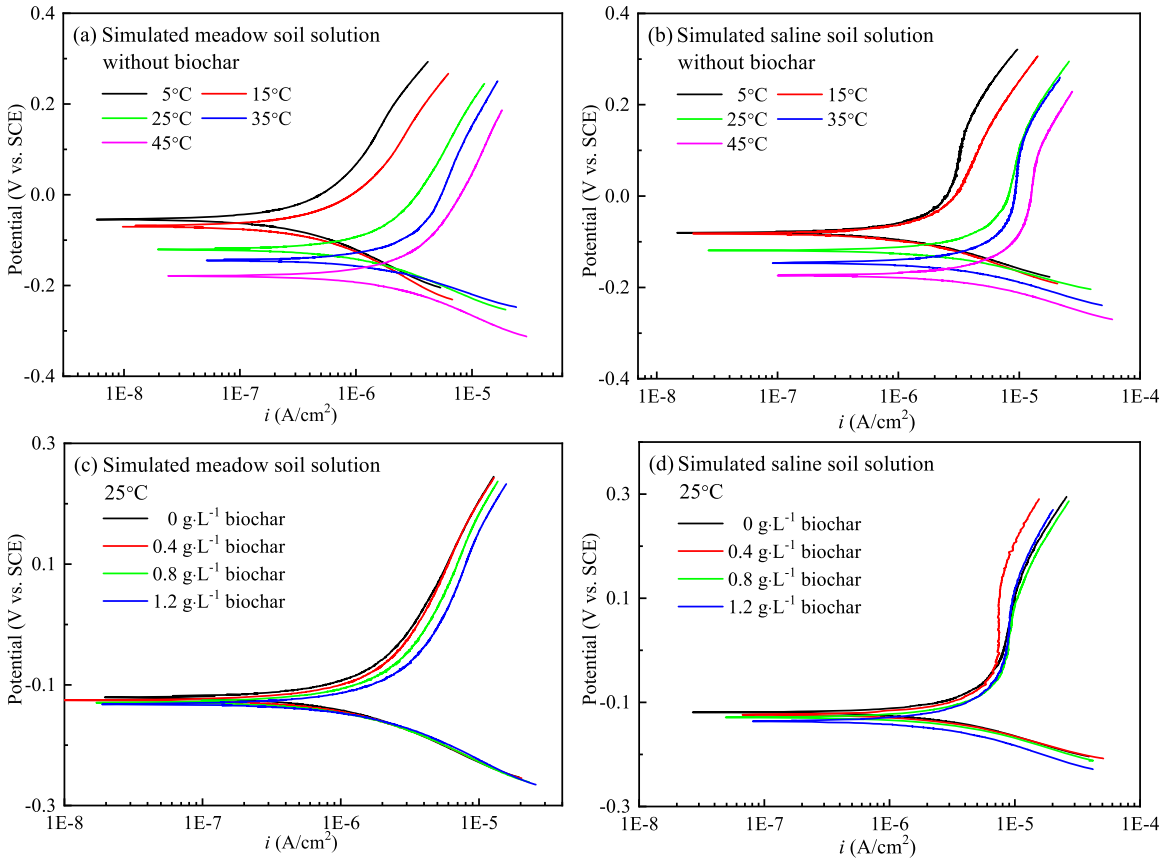

Figure 2. Polarization curves of arsenopyrite in simulated alkaline soil solutions at different temperatures without biochar (a, b) and at 25 °C with various biochar concentrations (c, d).

spectrum and the peak positions of the oxidation and reduction peaks under different conditions indicate that the change in temperature and the addition of biochar did not change the type of chemical reaction occurring at the arsenopyrite/electrolyte interface. However, increasing the temperatures (5, 15, 25, 35, and 45 °C) or the biochar concentration (0, 0.4, 0.8, and 1.2 g·L^{-1}) could promote the weathering process of arsenopyrite, as reflected by the larger current density in the CV plots (Figure 1). Furthermore, we found that the simulated saline soil solution had a larger rate of arsenopyrite weathering than the simulated meadow soil and that the influence of temperature on the weathering rate was more significant compared to biochar.

During the anodic scan, the first oxidation peak A1 appeared at approximately 250 mV, which corresponds to the preliminary oxidation dissolution of FeAsS (Reaction 1).[34] When the potential was scanned to 500−600 mV, the product of reaction 1 was further oxidized (A2, Reactions 2-4). After scanning in the reverse direction, three reduction peaks were successively detected at 350−400 mV (C1, Reaction 5),[35] 100−150 mV (C2, Reaction 6),[36] and −550 mV (C3, Reaction 7),[12] which were assigned to the reduction of oxides formed in the anodic scan. In particular, the C2 peak was more obvious in the simulated meadow soil solution than in the saline soil, which may be due to the lower pH of the meadow soil solution. At about −130 mV, oxidation peak A3 (Reaction 8) appeared in the forward scan of the potential switching, which can be attributed to the reverse reaction of reaction 7. Moreover, Figure 1 shows the imbalance of the current value between the oxidation and reduction processes, which also implies that most of the oxidation products of FeAsS are soluble.[37]

$$\text{A1: } FeAsS + 3H_2O \rightarrow AsO_3^{3-} + Fe^{2+} + S^0 + 6H^+ + 5e^- \quad (1)$$

$$\text{A2: } Fe^{2+} \rightarrow Fe^{3+} + e^- \quad (2)$$

$$S^0 + 4H_2O \rightarrow 8H^+ + SO_4^{2-} + 6e^- \quad (3)$$

$$AsO_3^{3-} + H_2O \rightarrow AsO_4^{3-} + 2H^+ + 2e^- \quad (4)$$

$$\text{C1: } Fe^{3+} + e^- \rightarrow Fe^{2+} \quad (5)$$

$$\text{C2: } AsO_4^{3-} + 2H^+ + 2e^- \rightarrow AsO_3^{3-} + H_2O \quad (6)$$

$$\text{C3: } S^0 + 2H^+ + 2e^- \rightarrow H_2S \quad (7)$$

$$\text{A3: } H_2S \rightarrow S^0 + 2H^+ + 2e^- \quad (8)$$

Polarization Curves and Dissolution Rate Study. Polarization curve technology is usually used to detect the corrosion rate and corrosion resistance of materials.[38] In this study, we obtained the corrosion potential (E_{corr}) and corrosion current density (i_{corr}) of arsenopyrite in a SAS solution through the polarization curve and further calculated the relevant kinetic and thermodynamic parameters during the weathering process. Figure 2 shows the polarization curves of arsenopyrite in SAS solutions without biochar at different temperatures and with various biochar concentrations. The fitting results, E_{corr} and i_{corr}, which are obtained by extrapolating the polarization curve, are listed in Table 1. Results show that the curve shifts

https://doi.org/10.1021/acs.est.2c09874
Environ. Sci. Technol. 2023, 57, 8373−8384

Table 1. Electrochemical Parameters of Arsenopyrite Electrodes in Simulated Alkaline Soil Solutions at Different Temperatures and Biochar Concentrations

Alkaline soil	Influence factors	T (°C)	$c_{biochar}$ (g·L^{-1})	E_{corr} (mV)	i_{corr} (μA·cm^{-2})	Dissolution rate (mol·m^{-2}·s^{-1})
Meadow	Temperature	5	0	−55.12	0.552	1.14 × 10^{-8}
		15	0	−70.67	0.910	1.89 × 10^{-8}
		25	0	−121.22	2.049	4.25 × 10^{-8}
		35	0	−146.56	3.147	6.52 × 10^{-8}
		45	0	−179.73	3.707	7.68 × 10^{-8}
	Concentration	25	0	−121.22	2.049	4.25 × 10^{-8}
		25	0.4	−125.74	2.233	4.63 × 10^{-8}
		25	0.8	−129.70	2.683	5.56 × 10^{-8}
		25	1.2	−133.53	3.082	6.39 × 10^{-8}
Saline	Temperature	5	0	−82.51	1.898	3.93 × 10^{-8}
		15	0	−83.75	2.458	5.09 × 10^{-8}
		25	0	−121.78	5.833	1.21 × 10^{-7}
		35	0	−149.06	7.577	1.57 × 10^{-7}
		45	0	−177.50	9.128	1.89 × 10^{-7}
	Concentration	25	0	−121.78	5.833	1.21 × 10^{-7}
		25	0.4	−127.11	6.329	1.31 × 10^{-7}
		25	0.8	−131.05	6.979	1.45 × 10^{-7}
		25	1.2	−139.18	7.378	1.53 × 10^{-7}

Table 2. Equivalent Circuit Model Parameters for Arsenopyrite in Simulated Alkaline Soil Solutions at Different Temperatures

Soil	Temp (°C)	CPE_f, Y_0 (S·cm^{-2}·s^n)	n	R_f (Ω·cm^2)	CPE_{dl}, Y_0 (S·cm^{-2}·s^n)	n	R_t (Ω·cm^2)	χ^2
Meadow	5	5.258 × 10^{-5}	0.754	4.843E4	9.326 × 10^{-5}	0.557	2.965E5	3.09 × 10^{-4}
	15	7.202 × 10^{-5}	0.763	7.759E3	1.805 × 10^{-5}	0.558	3.090E5	5.37 × 10^{-4}
	25	4.925 × 10^{-4}	0.587	4.946E3	3.644 × 10^{-4}	0.593	2.921E5	2.62 × 10^{-3}
	35	1.072 × 10^{-4}	0.764	3.100E3	3.997 × 10^{-4}	0.604	2.448E5	9.48 × 10^{-4}
	45	1.287 × 10^{-4}	0.731	2.209E3	7.839 × 10^{-4}	0.694	2.018E5	5.92 × 10^{-4}
Saline	5	6.439 × 10^{-5}	0.770	1.210E3	1.143 × 10^{-4}	0.633	2.858E5	7.80 × 10^{-4}
	15	7.561 × 10^{-5}	0.769	1.134E3	1.834 × 10^{-4}	0.577	2.291E5	4.93 × 10^{-4}
	25	2.543 × 10^{-4}	0.748	1.028E3	8.689 × 10^{-4}	0.632	2.032E5	2.32 × 10^{-3}
	35	1.573 × 10^{-4}	0.740	1.001E3	4.773 × 10^{-4}	0.637	1.112E5	8.30 × 10^{-5}
	45	1.910 × 10^{-4}	0.769	8.936E2	9.503 × 10^{-4}	0.659	6.721E4	6.97 × 10^{-4}

significantly to the lower right as the temperature increases, which means a lower E_{corr} and an increase in i_{corr} (Table 1). E_{corr} indicates the chemical stability of the mineral; the smaller the value of E_{corr}, the more unstable the minerals. The value of i_{corr} reflects the degree of corrosion rate, and the data show that the increase in temperature accelerates the weathering of arsenopyrite and arsenic released into the SAS solution.

As indicated by the data in Figure 2c,d and Table 1, the presence of biochar resulted in negative E_{corr} and larger i_{corr}, suggesting that biochar promoted the oxidative dissolution of arsenopyrite. These observations may be related to the redox activity of biochar, which can abiotic reduce Fe(III), and adsorb or bind Fe(III)/Fe(II) for its unique structure.[10,11,30] The reduction of Fe(III) promotes the anodic oxidation reaction of arsenopyrite because Fe(III) is one of the products of the anodic reaction. This decreases the formation of passivation films that contain the iron arsenate phase and iron (oxyhydr)oxide phase on the mineral surface. Such processes promoted the dissolution of arsenopyrite. By comparison, the $i_{corr,\ saline}$ was larger than the value of $i_{corr,\ meadow}$, reflecting that arsenopyrite had a faster weathering rate in saline soil solution.

Based on the Faraday formula and the value of i_{corr}, we calculated the release rate of arsenic from arsenopyrite weathering, thereby quantitatively estimating the degree of arsenic pollution of arsenopyrite polluted alkaline soil. The Faraday formula is $v = \frac{Mi_{corr}}{nF}$, where v is the As(III) release rate (g·m^{-2}·h^{-1}), n is the valence state, F is the Faraday constant (1 F = 26.80 A·h·mol^{-1}), and M is the arsenic atomic weight (g·mol^{-1}). Our results show that biochar enhanced the release rate of As(III) from both the simulated meadow soil solution (4.25 × 10^{-8} mol·m^{-2}·s^{-1} without biochar versus 6.39 × 10^{-8} mol·m^{-2}·s^{-1} with 1.2 g·L^{-1} biochar) and saline soil solution (1.21 × 10^{-7} mol·m^{-2}·s^{-1} without biochar versus 1.53 × 10^{-7} mol·m^{-2}·s^{-1} with 1.2 g·L^{-1} biochar). This suggests that the content of As entered into soil increased from 100.35 to 150.94 g for meadow soil and 285.67 to 361.33 g for saline soil, respectively, assuming taking 1 m^2 arsenopyrite and a year for example.

The polarization curves were further used to delineate the effect of biochar content on the oxidative dissolution of arsenopyrite in real alkaline soil leachates, real alkaline soil leachates with Cl$^-$ added (with the same Cl$^-$ content as the SAS solutions), and low-Cl$^-$ alkaline solutions (containing only Cl$^-$ and with the same content as real alkaline soil leachates) (Figure S1, Table S3). The i_{corr} values obtained in real soil leachates and real alkaline soil leachates with Cl$^-$ added were lower than that in the simulated solution, which may be due to the interference from the abundant Ca ions in real soil leachates (Table S2). The As released from the weathering of arsenopyrite could bind with Ca to form different kinds of arsenic−calcium deposits,[39,40] forming a passivating effect on the oxidation of mineral, thereby

https://doi.org/10.1021/acs.est.2c09874
Environ. Sci. Technol. 2023, 57, 8373−8384

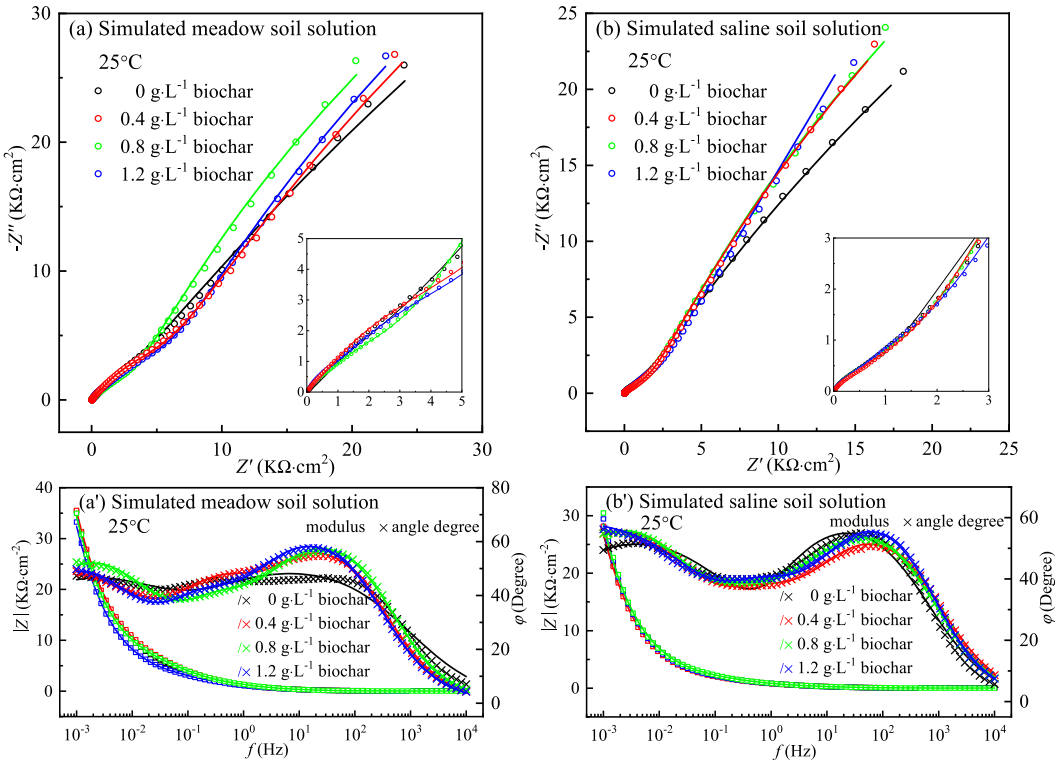

Figure 3. Nyquist (a, b) and Bode plots (a′, b′) for arsenopyrite in simulated alkaline soil solutions at different biochar concentrations at 25 °C, where ○, □, and × represent the experimental values and − represents the simulated values.

Table 3. Equivalent Circuit Model Parameters for Arsenopyrite in Simulated Alkaline Soil Solutions at Different Biochar Concentrations at 25 °C

Soil	$C_{biochar}$ (g·L^{-1})	CPE_f, Y_0 (S·cm^{-2}·s^n)	n	R_f (Ω·cm^2)	CPE_{al}, Y_0 (S·cm^{-2}·s^n)	n	R_{al} (Ω·cm^2)	CPE_{dl}, Y_0 (S·cm^{-2}·s^n)	n	R_t (Ω·cm^2)	χ^2
Meadow	0.4	3.895×10^{-4}	0.722	4607	2.341×10^{-4}	0.798	348.1	9.036×10^{-4}	0.681	2.175E5	3.56×10^{-4}
	0.8	4.397×10^{-4}	0.741	4554	2.013×10^{-4}	0.780	621.1	1.133×10^{-3}	0.719	1.878E5	1.48×10^{-4}
	1.2	5.052×10^{-4}	0.752	2217	2.031×10^{-4}	0.776	640.3	1.077×10^{-3}	0.708	1.832E5	2.77×10^{-4}
	0.4	6.633×10^{-4}	0.736	958	2.154×10^{-4}	0.720	320	1.329×10^{-3}	0.714	1.791E5	3.26×10^{-4}
Saline	0.8	7.584×10^{-4}	0.715	947	2.429×10^{-4}	0.723	413	1.308×10^{-3}	0.725	1.660E5	1.94×10^{-4}
	1.2	6.958×10^{-4}	0.711	934	1.309×10^{-4}	0.781	421	9.312×10^{-4}	0.655	1.624E5	4.32×10^{-4}

decreasing the weathering rate of arsenopyrite. Further, comparing the i_{corr} values in real soil leachates and low-Cl^- alkaline solutions, it can be found that the difference is not significant. This suggests that Cl^- is the most important factor affecting the weathering of arsenopyrite. However, all our results clearly show the significant role of biochar in promoting the oxidative dissolution of arsenopyrite in both SAS solutions and real soil leachates (Table S3).

Electrochemical Impedance Spectroscopy Study. Electrochemical impedance spectroscopy is a nondestructive analysis technique that can provide a variety of physical information on the electrode/solution interface such as surface passivation, mass transfer, kinetics, and reaction mechanisms.[41] Figure S2 presents the Nyquist and Bode plots for arsenopyrite in SAS solutions without biochar. The Bode diagram shows two time constants, consistent with the two capacitive loops of the Nyquist diagram. The capacitive loops at high-frequency were associated with pseudocapacitance and resistance of the surface passive layer, while the double-layer capacitance and charge transfer resistance of the mineral/solution interface corresponded to the capacitive loop at low frequency. For this reason, the equivalent circuit listed in Figure S3a was used to fit the EIS data at different temperatures without biochar, and the obtained fitted parameters are tabulated in Table 2. The χ^2 value, which lies on the order of 10^{-3}−10^{-5},[42] shows that the experimental data and the fitted value have a higher degree of agreement. R_s, R_f, and R_t in Figure S3a represent the solution resistance, passive film resistance, and charge transfer resistance, respectively. Due to the inhomogeneity and roughness of the electrode surface, constant phase elements CPE_f and CPE_{dl} were employed to replace the ideal capacitors of the surface passive film and double layer. By comparing the parameter values in Table 2, we found that the values of R_f and R_t decrease with increasing temperature, showing that the increase in temperature destroys the passivation film on the mineral surface and accelerates the transmission of ions, thereby expediting the weathering of arsenopyrite in SAS solutions.

Figure 3 shows the Nyquist and Bode plots for arsenopyrite in SAS solutions with various biochar concentrations. With soil solutions' presence of biochar, the Bode plots show another time constant, which may be attributed to the biochar adsorption layer. Inspection of Figure S3 plots with and without biochar indicated that there was an additional CPE_{al}

https://doi.org/10.1021/acs.est.2c09874
Environ. Sci. Technol. 2023, 57, 8373−8384

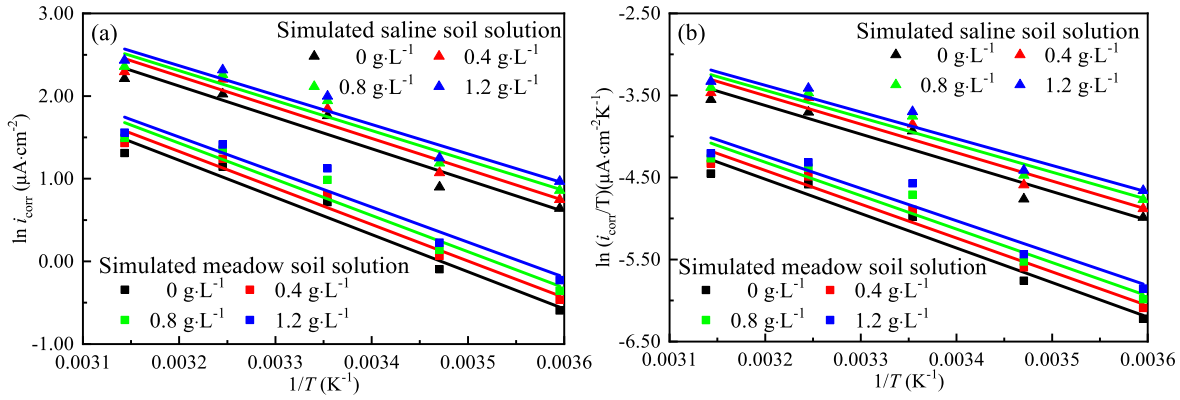

Figure 4. Relationship of ln i versus $1/T$ (a) and ln (i/T) versus $1/T$ (b) for arsenopyrite in simulated alkaline soil solutions without and with different biochar concentrations.

and R_{al}, which represent the capacitance and resistance of the biochar adsorption layer. The fitting results reflect that biochar significantly reduces R_f and R_t (Table 3). The decrease in R_f implies that the presence of biochar reduces the passivation effect of the film or hinders the production of the passivation layer, which is consistent with the results of the polarization curves. Additionally, the lower R_t predicts that the biochar enhances the ion transport on the mineral/solution interface. Although the R_{al} increased slightly with increasing biochar concentration, the total resistance (R_f + R_{al} + R_t) value gradually decreased; that is, the oxidation rate of arsenopyrite was accelerated by degrees. The EIS results of parallel experiments conducted in real soil leachates reflected trends consistent with those in the SAS solution (Figure S4, Table S4). In addition, the results of Tables 2 and 3 reveal that the weathering rate of arsenopyrite in the simulated saline soil solution was higher than that in the meadow soil, regardless of the presence of biochar. This is likely due to the higher Cl^- in the saline soil solution, which can destroy the passivation layer on the mineral surface and expedite the weathering process.[34] The EIS results can well explain the conclusions of the above polarization curves.

Activation Thermodynamic Parameters. To better visualize the effect of biochar on the weathering reaction of arsenopyrite, we calculated the activation energy (E_a) of the oxidation process of arsenopyrite in SAS solutions based on the following Arrhenius formula

$$\ln k = -\frac{E_a}{RT} + \ln A \tag{9}$$

where k is the weathering rate, R is the gas constant, T is the absolute temperature, and A is the frequency factor. Based on the Faraday's law mentioned above, it is clear that there is a proportional relationship between i_{corr} and k, so the i_{corr} (Tables 1 and S5, Figure S5) can be used instead of k and displays a linear curve of ln i_{corr} and $1/T$. After the linear regression of the curves (Figure 4a), the activation energy can be determined according to the slope of the curve. Table S6 demonstrates the E_a of arsenopyrite oxidation in the SAS solution at different biochar concentrations. The results manifested that higher biochar concentration reduced the E_a, demonstrating that biochar was beneficial for arsenopyrite oxidation. By comparison, the E_a of arsenopyrite oxidation in saline soil was always smaller than that in meadow soil under the same conditions, further confirming that arsenopyrite would occur more seriously eroded in saline soil.

According to reaction kinetic theory and the calculated activation energies (>20 kJ·mol^{-1}), the rate of arsenopyrite oxidation is controlled by surface interaction.[43] Further, the activation enthalpy (ΔH^*) of arsenopyrite weathering was calculated based on the transition state theory[44] and the drawn straight lines as shown in Figure 4b

$$\ln\left(\frac{k}{T}\right) = \left(\ln\left(\frac{R}{N_A h}\right) + \left(\frac{\Delta S^*}{R}\right)\right) - \frac{\Delta H^*}{RT} \tag{10}$$

where N_A is Avogadro's number, h is Planck's constant, and ΔS^* is the activation entropy. The result tabulated in Table S6 and the positive ΔH^* indicate that the weathering of arsenopyrite is an endothermic process, further confirming the notion that increasing the temperature can promote weathering. The presence of biochar also reduces the ΔH^* of the weathering reaction, which reduces the energy demand, making the weathering process easier to occur.

Surface Characterization. The Raman results (Figure S6) reveal that within the experimental temperature range, the oxidation products of iron arsenate and iron (oxyhydr)oxide (Reaction 11) could always be detected, regardless of biochar concentration. Consistent with previous studies, the presence of secondary phase products, ferric arsenate, and iron (oxyhydr)oxides hindered further oxidation of arsenopyrite.[5,45]

$$Fe^{3+} + 3OH^- \rightarrow FeOOH + H_2O \rightarrow 0.5\alpha - Fe_2O_3 + 1.5H_2O \tag{11}$$

For the raw biochar, FTIR spectra (Figure S7) show a sharp spectral band at 1600 cm^{-1}, which was assigned to the carboxyl C═O stretching vibration,[46] and aromatic C−C/C−O stretching of conjugated quinones.[47] The small peaks at 1385 and 1035 cm^{-1} were attributed to the −OH vibration of phenols and COO^-.[48,49] Three small but obvious peaks at 875, 815, and 750 cm^{-1} were ascribed to C−H bond vibrations in aromatic compounds.[49] The spectra show that after interactions between the biochar and metal ions, the peaks of organic functional groups underwent a shift in position or a change in peak intensity, which was due to the formation of organically metal complexes through ligand exchange or surface adsorption on biochar. In the biochar and Fe(III) systems, the shift of peak from 1035 to 1130 cm^{-1} suggests the formation of biochar-Fe complexes and the bending mode of Fe−OH.[50] In addition, a new peak appears at 600 cm^{-1}, which may be attributed to the formation of Fe−O bonds.[51] The peak at 1600 shifted slightly to 1615 cm^{-1} in the biochar and

https://doi.org/10.1021/acs.est.2c09874
Environ. Sci. Technol. 2023, 57, 8373−8384

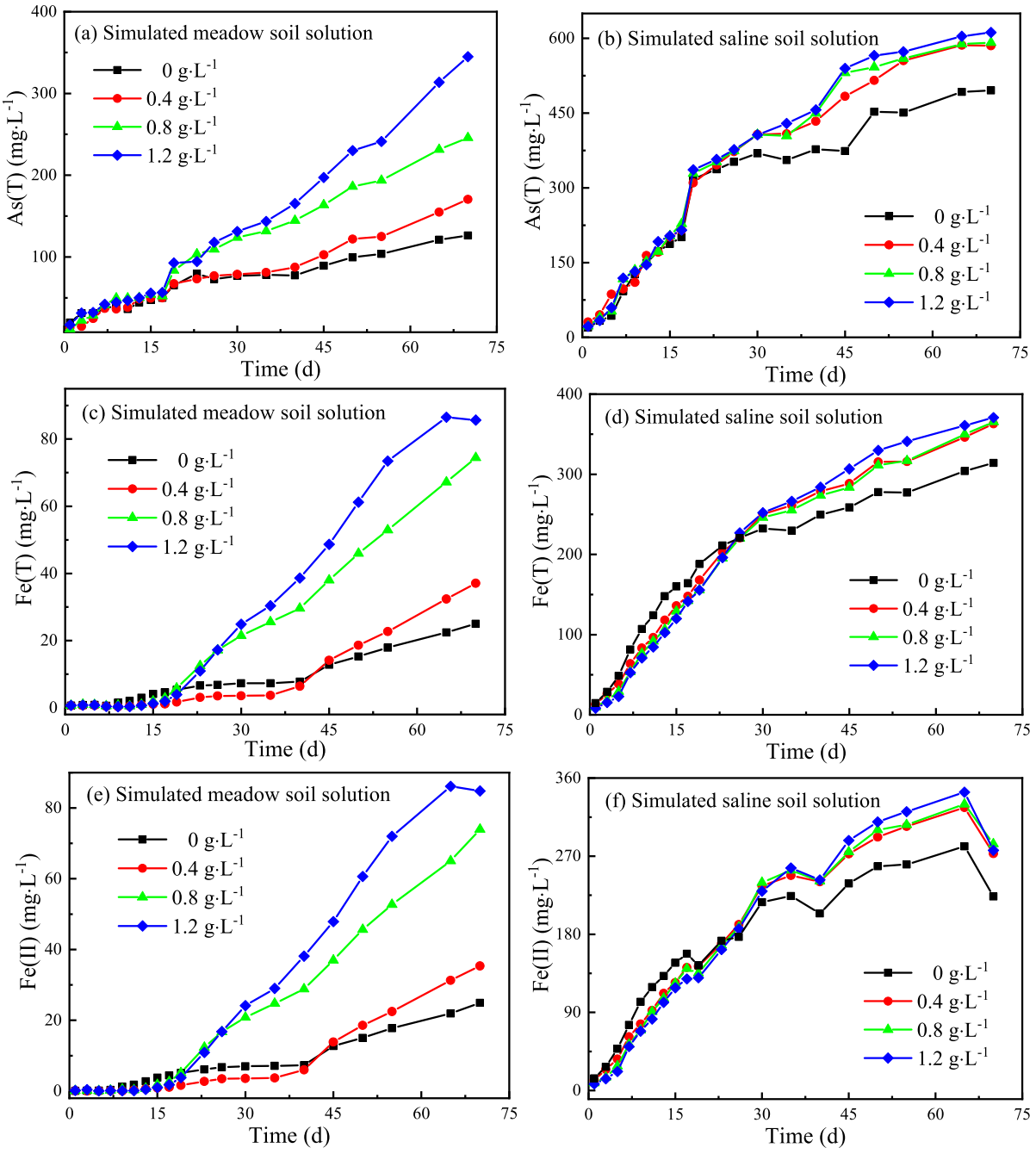

Figure 5. Changes of solution parameters during arsenopyrite oxidation in simulated alkaline soil solutions with the addition of different amounts of biochar. As(T) (a, b), Fe(T) (c, d), Fe(II) (e, f).

Fe(III)/As(V) systems, which may be due to the formation of biochar−Fe-As complexes via carboxyl groups. The appearance of a new peak at 827 cm^{-1} indicates the presence of As−O−Fe,[51,52] which could be the formation of amorphous iron arsenate or arsenate adsorbed on iron (oxyhydr)oxide. In the system with biochar and As(V), no shift in the peak position or appearance of new peaks was detected, implying little or no complexation or adsorption of arsenic on biochar. These observations confirmed that biochar can adsorb Fe ions in solution and that the presence of aromatic and quinoid groups in biochar could reduce Fe(III) (see details in the next section). Consequently, biochar reduces the content of Fe(III) in the solution, thereby impeding the production of passivation films, such as iron arsenate and iron (oxyhydr)oxide, and facilitating the oxidation and dissolution of arsenopyrite. The SEM (Figure S8) results also confirmed that the higher the concentration of biochar was, the rougher and more heterogeneous the surface of the mineral after weathering in solution.

To more intuitively determine the influence of temperature and biochar concentration changes on the oxidation degree of arsenopyrite, the XPS spectrum was carried out on the surface of the reacted arsenopyrite (Figures S9−S112, Tables S7−S9). The XPS spectra of pristine arsenopyrite (Figure S10a) show that the Fe species consists mainly of Fe(II)-AsS, Fe(III)-AsS, and Fe(III)-O, while the As species contains As(-I)-S, As(0), As(I)-O, As(III)-O, and As(V)-O, and for the S species it contains six chemical forms, identified as S^{2-}, $(AsS)^{2-}$, S_n^{2-}, S^0,

https://doi.org/10.1021/acs.est.2c09874
Environ. Sci. Technol. 2023, 57, 8373−8384

SO_3^{2-}, and SO_4^{2-}. Specifically, the dominant content of species for Fe, As, and S was that of the reduced state species, Fe(II)-AsS (68.39%), As(-I)-S (70.29%), and $(AsS)^{2-}$ (45.03%), respectively. This shows a slight oxidation of the surface of the pristine arsenopyrite in the air. The fitted result of Fe (Table S7), As (Table S8), and S (Table S9) attested that the content of oxidized species (Fe(III)-SO, As(V)-O, and SO_4^{2-}) gradually increased with increasing temperature and biochar concentration, indicating that the degree of oxidation on the surface of arsenopyrite gradually deepens. This is consistent with the electrochemical results showing that the elevated temperature and biochar concentration enhanced the i_{corr} and oxidation rate of arsenopyrite.

Immersion Test Analysis. In the separate immersion experiment, the amount of Fe(II) and Fe(III) remaining in the Fe(III) (Fe^{3+} = 300 mg·L^{-1}) solution after 24 h of biochar addition was measured. The results (Table S10) show that about half of the Fe(III) remained after reaction, and approximately 55 mg/L of dissolved Fe(II) was detected. Consistent with FTIR results, the immersion results show that biochar can reduce Fe(III), possibly act as an electron donor, and bind or adsorb Fe. This is likely due to the unique structural feature of biochar itself and the abundant redox-active functional groups,[9,53] including aromatic and quinone groups. To further verify the adsorption and reduction of As(V) on biochar, another immersion experiment was conducted. Results showed a very weak adsorption but a significant reduction of As(V) by biochar (Table S11).[54] These observations are consistent with the previous notion showing that unmodified or pristine biochar has little or no adsorption on As(V).[55]

The changes of As and Fe species in the liquid phase during the oxidation of arsenopyrite in SAS solutions are illustrated in Figures 5 and S13. It can be demonstrated that the addition of biochar significantly promoted the oxidative dissolution of arsenopyrite and the release of As(T) and As(III) into the ecological environment, exacerbating the As contamination, consistent with the electrochemical results as described above. The comparison of total As and total Fe content showed that biochar remarkably adsorbed Fe from the solution, while Fe(II) accounted for the majority of total Fe, which indicated the reduction and adsorption of Fe by biochar. The results (Figure S14) of leaching experiments in real soil leachates also showed that the addition of biochar promoted the weathering of arsenopyrite, facilitating arsenic migration and contamination.

Figure S15(a, b) and Figure S15(c, d) show the variation in pH with time during arsenopyrite power leaching in the SAS solutions and real soil leachate without/with 1.2 g·L^{-1} biochar, respectively. Compared to the SAS solution, the pH change in the real leachate was clearly lower, e.g. in the real meadow soil leachate, the pH initially decreased and then returned to the original value. This is attributed to the fact that the natural organic matter in the soil acts as a natural buffer and potentially controls the pH.[56] However, the aforementioned polarization curve test still proved that the existence of biochar could intensify the oxidation of arsenopyrite in the real soil leachate. The process of arsenopyrite oxidation in a neutral environment involves multiple steps and intermediate products. In the simulated meadow soil solution (Figure S15a), there was a slight increase in pH after about 30 min of the initial reaction, which could be due to the consumption of hydrogen ions in the oxidation of Fe(II) to Fe(III). However, the pH drops due to release of protons are conducive to the subsequent transformation of Fe(III) to iron (oxyhydr)oxide and the oxidation of S^0 to SO_3^{2-} and SO_4^{2-}.[57] It can be found that the pH change in the meadow soil solution is gentler than that in the saline (Figure S15b), which may be attributed to the bicarbonate (0.11 g·L^{-1}) as a pH buffer in the simulated meadow soil solution. In contrast, the higher Cl^- (1.81 g·L^{-1}) ion concentration destroys the passivation film on the surface and promotes the dissolution of minerals, resulting in a lower pH in saline soil solutions. Furthermore, the addition of biochar enhanced the weathering of arsenopyrite and lowered the pH of the solution, which aggravates hydrogen ion pollution in the surrounding environment.

Weathering Mechanism of Arsenopyrite in the Absence/Presence of Biochar. According to electrochemical measurements, immersion tests, and surface characterization, this study demonstrated the effect of biochar on arsenopyrite weathering in simulated alkaline soil solutions and real alkaline soil leachates and summarized the corresponding weathering mechanism (Figure 6). In the absence of biochar,

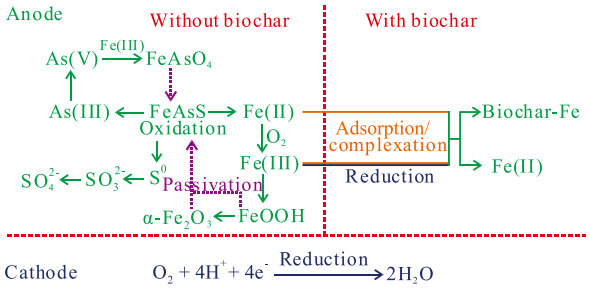

Figure 6. Scheme of the weathering mechanism for arsenopyrite in alkaline soil solutions.

the As and Fe ions released by the oxidation of arsenopyrite could generate iron arsenate ($FeAsO_4$) adhering to the surface of the mineral. In addition, the Fe(III) ions were also partially converted to iron (oxyhydr)oxide (FeOOH and α-Fe_2O_3) under weak alkaline conditions. The formation of iron arsenate and iron (oxyhydr)oxide inhibited the oxidative dissolution of arsenopyrite. In stark contrast, the presence of biochar reduced Fe(III) and As(V) along with the adsorption of Fe ions owing to its redox activity and special physical structure, thus diminishing the loading of iron used to generate the passivation film. The decrease of passivation film, including iron arsenate and iron (oxyhydr)oxide, not only reduces the adsorption of arsenic but also more significantly expedites the weathering of arsenopyrite.

Environmental Implication. This study proposes a new environmental process, that is, biochar accelerates the release of arsenic in soil. Biochar has the redox activity of reducing Fe(III) and As(V), perhaps as an electron donor, and can adsorb iron to decrease the content of iron. Therefore, it suppressed the formation of the passivation layer, such as iron arsenate and iron (oxyhydr)oxide, which significantly promotes the oxidative dissolution of arsenopyrite and arsenic release. Our results extend the knowledge of the effect of biochar on arsenic migration and transformation. Previous studies have confirmed that biochar can promote the reductive dissolution of iron (oxyhydr)oxides that can adsorb arsenic,[58,59] and the inherent components of biochar, including dissolved organic carbon, silicates, and phosphate,[60,61] can directly compete with

https://doi.org/10.1021/acs.est.2c09874
Environ. Sci. Technol. 2023, 57, 8373−8384

oxyanion arsenic on iron (oxyhydr)oxide for adsorption, thus enhancing the mobility and boosting the liberation of arsenic into the soil and water. Furthermore, our study not only substantiated the promoting effect of biochar on the weathering dissolution of arsenopyrite as the main arsenic source but also quantitatively calculated the amount of arsenic released under different biochar concentrations. The activation thermodynamic parameters, E_a and ΔH^*, for arsenopyrite oxidation calculated by electrochemical methods showed a continuous decrease with increasing concentrations of coexisting biochar. The successful application of electrochemical technology in this study provides a meaningful and reference means for solving similar environmental problems. While the arsenopyrite weathering rate was larger in the simulated alkaline soil solutions than the real alkaline soil leachates, our results clearly demonstrate the critical role of biochar in promoting the weathering of arsenopyrite under the conditions tested. The higher weathering rate of arsenopyrite in the SAS solution compared to real soil leachates is likely due to the presence of high Cl^- in SAS solutions, which destroy the passivation layer on the mineral surface. In addition to Cl^-, other factors, such as microorganisms and multiple cations in real soil environment, could also affect the interaction of biochar with arsenopyrite. Future study is required to examine the effect of biochar on the oxidation mechanism of arsenopyrite and, more importantly, on the release and transport of arsenic in the actual soil environments under the coupling of multiple variable factors.

■ ASSOCIATED CONTENT

Supporting Information

P(PDF). The Supporting Information is available free of charge at https://pubs.acs.org/doi/10.1021/acs.est.2c09874.

Polarization curves of arsenopyrite in real alkaline soil leachates, Nyquist and Bode plots for arsenopyrite, equivalent circuit for arsenopyrite, polarization curves, Raman, FTIR, SEM, and XPS characterizations, detailed experimental and electrochemical parameters (PDF)

■ AUTHOR INFORMATION

Corresponding Author

Qingyou Liu − *Key Laboratory of High-temperature and High-pressure Study of the Earth's Interior, Institute of Geochemistry, Chinese Academy of Sciences, Guiyang 550081, China;* orcid.org/0000-0002-5630-7680; Email: liuqingyou@vip.gyig.ac.cn

Authors

Shuai Wang − *Key Laboratory of High-temperature and High-pressure Study of the Earth's Interior, Institute of Geochemistry, Chinese Academy of Sciences, Guiyang 550081, China; University of Chinese Academy of Sciences, Beijing 100039, China*

Peng Liao − *State Key Laboratory of Environmental Geochemistry, Institute of Geochemistry, Chinese Academy of Sciences, Guiyang 550081, China;* orcid.org/0000-0001-6924-1097

Ling Cen − *Key Laboratory of High-temperature and High-pressure Study of the Earth's Interior, Institute of Geochemistry, Chinese Academy of Sciences, Guiyang 550081, China; University of Chinese Academy of Sciences, Beijing 100039, China*

Hongguang Cheng − *State Key Laboratory of Environmental Geochemistry, Institute of Geochemistry, Chinese Academy of Sciences, Guiyang 550081, China*

Complete contact information is available at: https://pubs.acs.org/10.1021/acs.est.2c09874

Author Contributions

S.W. and P.L. contributed equally to this work.

Notes

The authors declare no competing financial interest.

■ ACKNOWLEDGMENTS

This work was financially supported by the National Key Research and Development Program of China (2018YFC1802601), the National Natural Science Foundation of China (41873074) and the Innovation and Entrepreneurship Talents of Guizhou Province (NO GZQ202208091).

■ REFERENCES

(1) Kumarathilaka, P.; Seneweera, S.; Meharg, A.; Bundschuh, J. Arsenic speciation dynamics in paddy rice soil-water environment: sources, physico-chemical, and biological factors - A review. *Water Res.* **2018**, *140*, 403−414.

(2) Yu, Y.; Zhu, Y.; Gao, Z.; Gammons, C. H.; Li, D. Rates of arsenopyrite oxidation by oxygen and Fe(III) at pH 1.8−12.6 and 15−45 degrees C. *Environ. Sci. Technol.* **2007**, *41* (18), 6460−4.

(3) Biswas, A.; Besold, J.; Sjöstedt, C.; Gustafsson, J. P.; Scheinost, A. C.; Planer-Friedrich, B. Complexation of Arsenite, Arsenate, and Monothioarsenate with Oxygen-Containing Functional Groups of Natural Organic Matter: An XAS Study. *Environ. Sci. Technol.* **2019**, *53* (18), 10723−10731.

(4) Zhang, P.; Yao, W.; Yuan, S. Citrate-enhanced release of arsenic during pyrite oxidation at circumneutral conditions. *Water Res.* **2017**, *109*, 245−252.

(5) Battistel, M.; Stolze, L.; Muniruzzaman, M.; Rolle, M. Arsenic release and transport during oxidative dissolution of spatially-distributed sulfide minerals. *J. Hazard. Mater.* **2021**, *409*, 124651.

(6) Li, S.; Harris, S.; Anandhi, A.; Chen, G. Predicting biochar properties and functions based on feedstock and pyrolysis temperature: A review and data syntheses. *J. Clean. Prod.* **2019**, *215*, 890−902.

(7) Lian, F.; Xing, B. Black Carbon (Biochar) In Water/Soil Environments: Molecular Structure, Sorption, Stability, and Potential Risk. *Environ. Sci. Technol.* **2017**, *51* (23), 13517−13532.

(8) Klüpfel, L.; Keiluweit, M.; Kleber, M.; Sander, M. Redox Properties of Plant Biomass-Derived Black Carbon (Biochar). *Environ. Sci. Technol.* **2014**, *48* (10), 5601−5611.

(9) Kim, H. B.; Kim, S. H.; Jeon, E. K.; Kim, D. H.; Tsang, D. C. W.; Alessi, D. S.; Kwon, E. E.; Baek, K. Effect of dissolved organic carbon from sludge, Rice straw and spent coffee ground biochar on the mobility of arsenic in soil. *Sci. Total Environ.* **2018**, *636*, 1241−1248.

(10) Xu, S.; Adhikari, D.; Huang, R.; Zhang, H.; Tang, Y.; Roden, E.; Yang, Y. Biochar-Facilitated Microbial Reduction of Hematite. *Environ. Sci. Technol.* **2016**, *50* (5), 2389−95.

(11) Kappler, A.; Wuestner, M. L.; Ruecker, A.; Harter, J.; Halama, M.; Behrens, S. Biochar as an Electron Shuttle between Bacteria and Fe(III) Minerals. *Environ. Sci. Technol. Lett.* **2014**, *1* (8), 339−344.

(12) Liu, X. L.; Li, Q.; Zhang, Y.; Jiang, T.; Yang, Y. B.; Xu, B.; He, Y. H. Electrochemical behaviour of the dissolution and passivation of arsenopyrite in 9K culture medium. *Appl. Surf. Sci.* **2020**, *508*, 145269.

(13) Deng, S.; Gu, G. An electrochemical impedance spectroscopy study of arsenopyrite oxidation in the presence of Sulfobacillus thermosulfidooxidans. *Electrochim. Acta* **2018**, *287*, 106−114.

(14) Corkhill, C. L.; Vaughan, D. J. Arsenopyrite oxidation − A review. *Appl. Geochem.* **2009**, *24* (12), 2342−2361.

(15) Wang, S.; Jiao, B.; Zhang, M.; Zhang, G.; Wang, X.; Jia, Y. Arsenic release and speciation during the oxidative dissolution of arsenopyrite by O_2 in the absence and presence of EDTA. *J. Hazard. Mater.* **2018**, *346*, 184−190.
(16) Lara, R. H.; Velazquez, L. J.; Vazquez-Arenas, J.; Mallet, M.; Dossot, M.; Labastida, I.; Sosa-Rodriguez, F. S.; Espinosa-Cristobal, L. F.; Escobedo-Bretado, M. A.; Cruz, R. Arsenopyrite weathering under conditions of simulated calcareous soil. *Environ. Sci. Pollut. Res.* **2016**, *23* (4), 3681−706.
(17) Hong, J.; Liu, L.; Tan, W.; Qiu, G. Arsenic release from arsenopyrite oxidative dissolution in the presence of citrate under UV irradiation. *Sci. Total Environ.* **2020**, *726*, 138429.
(18) Zhang, D. R.; Chen, H. R.; Xia, J. L.; Nie, Z. Y.; Fan, X. L.; Liu, H. C.; Zheng, L.; Zhang, L. J.; Yang, H. Y. Humic acid promotes arsenopyrite bio-oxidation and arsenic immobilization. *J. Hazard. Mater.* **2020**, *384*, 121359.
(19) Wang, S.; Zheng, K.; Li, H.; Feng, X.; Wang, L.; Liu, Q. Arsenopyrite weathering in acidic water: Humic acid affection and arsenic transformation. *Water Res.* **2021**, *194*, 116917.
(20) Saifullah; Dahlawi, S.; Naeem, A.; Rengel, Z.; Naidu, R. Biochar application for the remediation of salt-affected soils: Challenges and opportunities. *Sci. Total Environ.* **2018**, *625*, 320−335.
(21) Zheng, N.; Yu, Y.; Li, Y.; Ge, C.; Chapman, S. J.; Yao, H. Can aged biochar offset soil greenhouse gas emissions from crop residue amendments in saline and non-saline soils under laboratory conditions? *Sci. Total Environ.* **2022**, *806* (Pt 3), 151256.
(22) Zhou, Z.; Li, Z.; Zhang, Z.; You, L.; Xu, L.; Huang, H.; Wang, X.; Gao, Y.; Cui, X. Treatment of the saline-alkali soil with acidic corn stalk biochar and its effect on the sorghum yield in western Songnen Plain. *Sci. Total Environ.* **2021**, *797*, 149190.
(23) Rafiq, M. K.; Bai, Y.; Aziz, R.; Rafiq, M. T.; Masek, O.; Bachmann, R. T.; Joseph, S.; Shahbaz, M.; Qayyum, A.; Shang, Z.; Danaee, M.; Long, R. Biochar amendment improves alpine meadows growth and soil health in Tibetan plateau over a three year period. *Sci. Total Environ.* **2020**, *717*, 135296.
(24) Mandaliev, P. N.; Mikutta, C.; Barmettler, K.; Kotsev, T.; Kretzschmar, R. Arsenic species formed from arsenopyrite weathering along a contamination gradient in Circumneutral river floodplain soils. *Environ. Sci. Technol.* **2014**, *48* (1), 208−17.
(25) Robson, T. C.; Braungardt, C. B.; Keith-Roach, M. J.; Rieuwerts, J. S.; Worsfold, P. J. Impact of arsenopyrite contamination on agricultural soils and crops. *Journal of Geochemical Exploration* **2013**, *125*, 102−109.
(26) Mihaljevic, M.; Ettler, V.; Sebek, O.; Drahota, P.; Strnad, L.; Prochazka, R.; Zeman, J.; Sracek, O. Alteration of arsenopyrite in soils under different vegetation covers. *Sci. Total Environ.* **2010**, *408* (6), 1286−94.
(27) Cheng, H.; Jones, D. L.; Hill, P.; Bastami, M. S.; Tu, C. l. Influence of biochar produced from different pyrolysis temperature on nutrient retention and leaching. *Archives of Agronomy and Soil Science* **2018**, *64* (6), 850−859.
(28) Lin, B.; Lu, X.; Li, L. Electrochemical corrosion behavior of arc sprayed Zn and Zn15Al coatings in simulated salina soil and neutral meadow soil solutions. *Journal of Wuhan University of Technology-Mater. Sci. Ed.* **2011**, *26* (6), 1152−1156.
(29) Viollier, E.; Inglett, P. W.; Hunter, K.; Roychoudhury, A. N.; Van Cappellen, P. The ferrozine method revisited: Fe(II)/Fe(III) determination in natural waters. *Appl. Geochem.* **2000**, *15* (6), 785−790.
(30) Xu, J.; Yin, Y.; Tan, Z.; Wang, B.; Guo, X.; Li, X.; Liu, J. Enhanced removal of Cr(VI) by biochar with Fe as electron shuttles. *J. Environ. Sci.* **2019**, *78*, 109−117.
(31) Chen, Z.; Wang, Y.; Xia, D.; Jiang, X.; Fu, D.; Shen, L.; Wang, H.; Li, Q. B. Enhanced bioreduction of iron and arsenic in sediment by biochar amendment influencing microbial community composition and dissolved organic matter content and composition. *J. Hazard. Mater.* **2016**, *311*, 20−9.
(32) Corkhill, C. L.; Wincott, P. L.; Lloyd, J. R.; Vaughan, D. J. The oxidative dissolution of arsenopyrite (FeAsS) and enargite (Cu3AsS4) by Leptospirillum ferrooxidans. *Geochim. Cosmochim. Acta* **2008**, *72* (23), 5616−5633.
(33) Bonnissel-Gissinger, P.; Alnot, M.; Ehrhardt, J.-J.; Behra, P. Surface Oxidation of Pyrite as a Function of pH. *Environ. Sci. Technol.* **1998**, *32* (19), 2839−2845.
(34) Zheng, K.; Li, H.; Wang, S.; Feng, X.; Wang, L.; Liu, Q. Arsenopyrite weathering in sodium chloride solution: Arsenic geochemical evolution and environmental effects. *J. Hazard. Mater.* **2020**, *392*, 122502.
(35) Tu, Z.; Wan, J.; Guo, C.; Fan, C.; Zhang, T.; Lu, G.; Reinfelder, J. R.; Dang, Z. Electrochemical oxidation of pyrite in pH 2 electrolyte. *Electrochim. Acta* **2017**, *239*, 25−35.
(36) Almeida, C. M. V. B.; Giannetti, B. F. Electrochemical study of arsenopyrite weathering. *Phys. Chem. Chem. Phys.* **2003**, *5* (3), 604−610.
(37) Velásquez, P.; Leinen, D.; Pascual, J.; Ramos-Barrado, J. R.; Grez, P.; Gómez, H.; Schrebler, R.; Del Río, R.; Córdova, R. A Chemical, Morphological, and Electrochemical (XPS, SEM/EDX, CV, and EIS) Analysis of Electrochemically Modified Electrode Surfaces of Natural Chalcopyrite (CuFeS2) and Pyrite (FeS2) in Alkaline Solutions. *J. Phys. Chem. B* **2005**, *109* (11), 4977−4988.
(38) Mansfeld, F. Tafel slopes and corrosion rates obtained in the pre-Tafel region of polarization curves. *Corros. Sci.* **2005**, *47* (12), 3178−3186.
(39) Moon, D. H.; Dermatas, D.; Menounou, N. Arsenic immobilization by calcium-arsenic precipitates in lime treated soils. *Sci. Total Environ.* **2004**, *330* (1−3), 171−85.
(40) Bothe, J. V.; Brown, P. W. Arsenic Immobilization by Calcium Arsenate Formation. *Environ. Sci. Technol.* **1999**, *33* (21), 3806−3811.
(41) Mahato, P.; Mishra, S. K.; Murmu, M.; Murmu, N. C.; Hirani, H.; Banerjee, P. A prolonged exposure of Ti-Si-B-C nanocomposite coating in 3.5 wt% NaCl solution: Electrochemical and morphological analysis. *Surf. Coat. Technol.* **2019**, *375*, 477−488.
(42) Murmu, M.; Saha, S. K.; Murmu, N. C.; Banerjee, P. Effect of stereochemical conformation into the corrosion inhibitive behaviour of double azomethine based Schiff bases on mild steel surface in 1 mol L−1 HCl medium: An experimental, density functional theory and molecular dynamics simulation study. *Corros. Sci.* **2019**, *146*, 134−151.
(43) Lasaga, A. C. *Kinetic Theory in the Earth Sciences*; Princeton Series in Geochemistry; Princeton University Press: Princeton, NJ, 1998; Vol. *402*.
(44) Hegazy, M. A.; El-Tabei, A. S.; Bedair, A. H.; Sadeq, M. A. An investigation of three novel nonionic surfactants as corrosion inhibitor for carbon steel in 0.5M H2SO4. *Corros. Sci.* **2012**, *54*, 219−230.
(45) Hong, J.; Liu, L.; Ning, Z.; Liu, C.; Qiu, G. Synergistic oxidation of dissolved As(III) and arsenopyrite in the presence of oxygen: Formation and function of reactive oxygen species. *Water Res.* **2021**, *202*, 117416.
(46) Li, Z.; Sun, Y.; Yang, Y.; Han, Y.; Wang, T.; Chen, J.; Tsang, D. C. W. Biochar-supported nanoscale zero-valent iron as an efficient catalyst for organic degradation in groundwater. *J. Hazard. Mater.* **2020**, *383*, 121240.
(47) Tomczyk, A.; Sokołowska, Z.; Boguta, P. Biochar physicochemical properties: pyrolysis temperature and feedstock kind effects. *Rev. Environ. Sci. Biotechnol.* **2020**, *19* (1), 191−215.
(48) Amir, S.; Jouraiphy, A.; Meddich, A.; El Gharous, M.; Winterton, P.; Hafidi, M. Structural study of humic acids during composting of activated sludge-green waste: elemental analysis, FTIR and 13C NMR. *J. Hazard. Mater.* **2010**, *177* (1−3), 524−9.
(49) Niazi, N. K.; Bibi, I.; Shahid, M.; Ok, Y. S.; Shaheen, S. M.; Rinklebe, J.; Wang, H.; Murtaza, B.; Islam, E.; Farrakh Nawaz, M.; Luttge, A. Arsenic removal by Japanese oak wood biochar in aqueous solutions and well water: Investigating arsenic fate using integrated spectroscopic and microscopic techniques. *Sci. Total Environ.* **2018**, *621*, 1642−1651.
(50) Sharma, P.; Ofner, J.; Kappler, A. Formation of binary and ternary colloids and dissolved complexes of organic matter. *Fe and As. Environ. Sci. Technol.* **2010**, *44* (12), 4479−85.

https://doi.org/10.1021/acs.est.2c09874
Environ. Sci. Technol. 2023, 57, 8373−8384

(51) Zhang, D. R.; Chen, H. R.; Xia, J. L.; Nie, Z. Y.; Zhang, R. Y.; Schippers, A.; Shu, W. S.; Qian, L. X. Red mud regulates arsenic fate at acidic pH via regulating arsenopyrite bio-oxidation and S, Fe, Al, Si speciation transformation. *Water Res.* **2021**, *203*, 117539.
(52) Jia, Y.; Xu, L.; Wang, X.; Demopoulos, G. P. Infrared spectroscopic and X-ray diffraction characterization of the nature of adsorbed arsenate on ferrihydrite. *Geochim. Cosmochim. Acta* **2007**, *71* (7), 1643−1654.
(53) Park, J. H.; Lamb, D.; Paneerselvam, P.; Choppala, G.; Bolan, N.; Chung, J. W. Role of organic amendments on enhanced bioremediation of heavy metal(loid) contaminated soils. *J. Hazard. Mater.* **2011**, *185* (2−3), 549−74.
(54) Ahmad, M.; Rajapaksha, A. U.; Lim, J. E.; Zhang, M.; Bolan, N.; Mohan, D.; Vithanage, M.; Lee, S. S.; Ok, Y. S. Biochar as a sorbent for contaminant management in soil and water: A review. *Chemosphere* **2014**, *99*, 19−33.
(55) Hu, X.; Ding, Z.; Zimmerman, A. R.; Wang, S.; Gao, B. Batch and column sorption of arsenic onto iron-impregnated biochar synthesized through hydrolysis. *Water Res.* **2015**, *68*, 206−216.
(56) Zheng, J.; Berns-Herrboldt, E. C.; Gu, B.; Wullschleger, S. D.; Graham, D. E. Quantifying pH buffering capacity in acidic, organic-rich Arctic soils: Measurable proxies and implications for soil carbon degradation. *Geoderma* **2022**, *424*, 116003.
(57) Ferreira, P. M.; Majuste, D.; Freitas, E. T. F.; Caldeira, C. L.; Dantas, M. S. S.; Ciminelli, V. S. T. Galvanic effect of pyrite on arsenic release from arsenopyrite dissolution in oxygen-depleted and oxygen-saturated circumneutral solutions. *J. Hazard. Mater.* **2021**, *412*, 125236.
(58) Zhang, D.; Cao, R.; Wang, Y.; Wang, S.; Jia, Y. The adsorption of As(V) on poorly crystalline Fe oxyhydroxides, revisited: Effect of the reaction media and the drying treatment. *J. Hazard. Mater.* **2021**, *416*, 125863.
(59) Wu, X.; Bowers, B.; Kim, D.; Lee, B.; Jun, Y. S. Dissolved Organic Matter Affects Arsenic Mobility and Iron(III) (hydr)oxide Formation: Implications for Managed Aquifer Recharge. *Environ. Sci. Technol.* **2019**, *53* (24), 14357−14367.
(60) Zhong, D.; Ren, S.; Dong, X.; Yang, X.; Wang, L.; Chen, J.; Zhao, Z.; Zhang, Y.; Tsang, D. C. W.; Crittenden, J. C. Rice husk-derived biochar can aggravate arsenic mobility in ferrous-rich groundwater during oxygenation. *Water Res.* **2021**, *200*, 117264.
(61) Muehe, E. M.; Scheer, L.; Daus, B.; Kappler, A. Fate of Arsenic during Microbial Reduction of Biogenic versus Abiogenic As−Fe(III)−Mineral Coprecipitates. *Environ. Sci. Technol.* **2013**, *47* (15), 8297−8307.

https://doi.org/10.1021/acs.est.2c09874
Environ. Sci. Technol. 2023, 57, 8373−8384